U.S. DEPARTMENT OF THE INTERIOR
U.S. GEOLOGICAL SURVEY

Prepared for the
NATIONAL AERONAUTICS AND SPACE ADMINISTRATION

GEOLOGIC MAP OF THE BARRYMORE QUADRANGLE (V–59), VENUS

By
Jeffrey R. Johnson, Goro Komatsu, and Victor R. Baker

1999

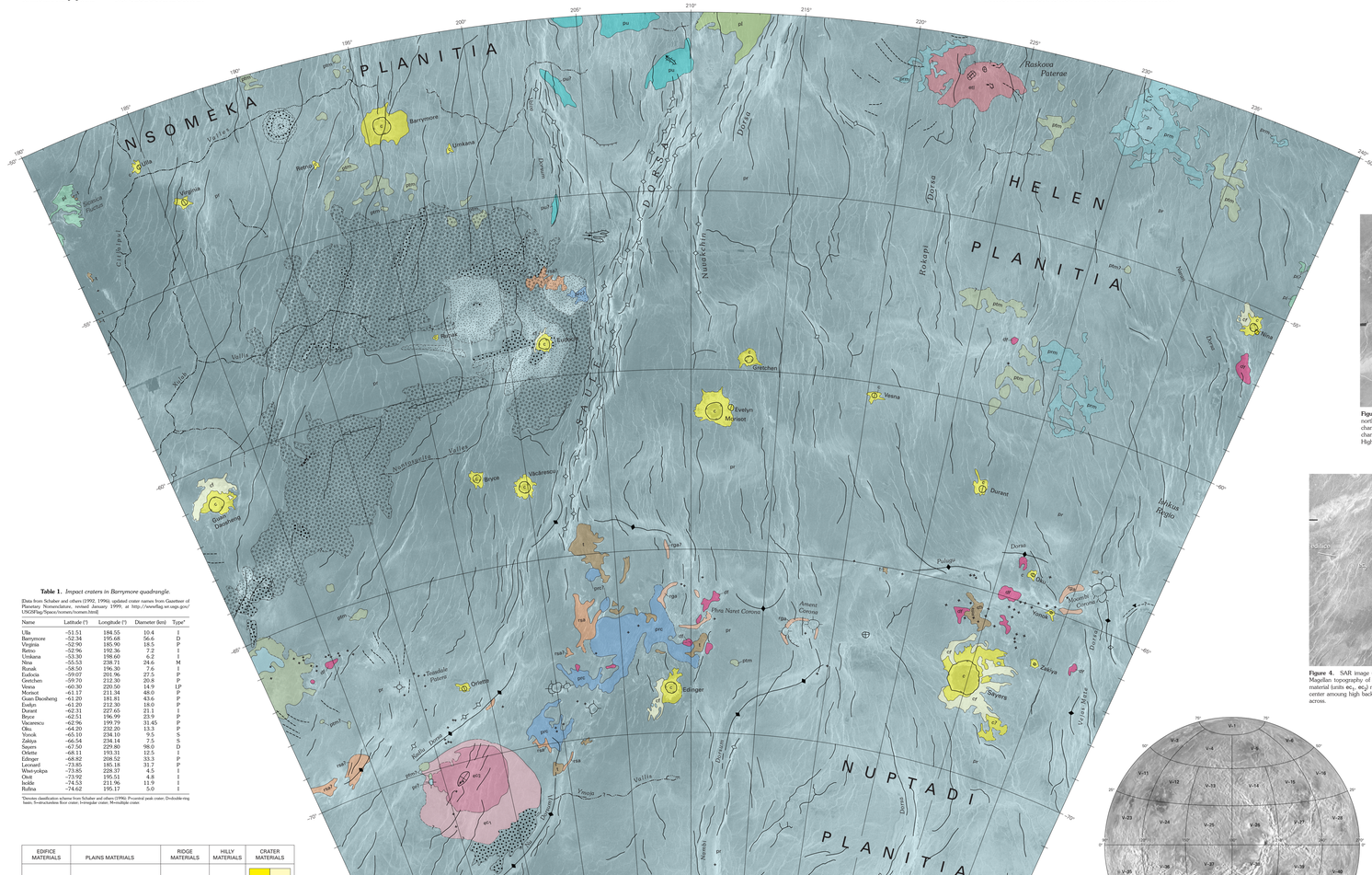

Table 1. *Impact craters in Barrymore quadrangle.*

[Data from Schaber and others (1992, 1996); updated crater names from Gazetteer of Planetary Nomenclature, revised January 1999, at http://wwwflag.wr.usgs.gov/USGSFlag/Space/venus/venmen.html]

Name	Latitude (°)	Longitude (°)	Diameter (km)	Type[a]
Ulla	–51.51	184.55	10.4	I
Barrymore	–52.34	195.68	56.6	D
Virginia	–52.90	185.90	18.5	P
Rerva	–52.96	192.36	7.2	I
Urokana	–53.30	198.60	6.2	I
Nina	–53.50	178.70	14.4	M
Ila	–58.50	196.30	7.6	I
Eudocia	–59.07	201.96	27.5	P
Gretchen	–59.70	212.30	20.8	P
Vesna	–60.30	220.50	14.9	LP
Morisot	–61.17	211.34	48.0	P
Guan Daosheng	–61.20	181.81	43.6	P
Evelyn	–61.20	212.30	18.0	P
Durant	–62.31	227.65	21.1	I
Bryce	–62.51	196.99	23.9	P
Vlacrescu	–62.96	199.79	31.45	P
Ulla	–64.20	232.20	13.3	P
Yonoh	–65.10	234.10	9.5	S
Zakiya	–66.54	234.14	7.5	S
Sayers	–67.50	229.80	98.0	D
Ortelius	–68.10	208.12	12.1	I
Edinger	–69.42	224.52	33.3	P
Tolstoi	–73.85	195.18	14.7	P
Wise-yakpa	–73.85	229.37	4.5	I
Otoi	–73.92	195.51	4.8	I
Isolde	–74.53	211.96	11.9	I
Rufina	–74.62	195.17	5.0	I

[a]Denotes classification scheme from Schaber and others (1996): P=central peak crater, D=double-ring basin, S=whatchamacallum floor crater, I=irregular crater, M=multiple crater.

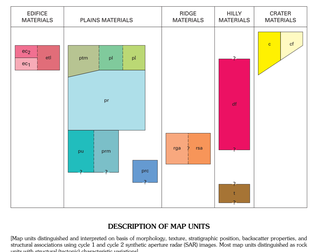

DESCRIPTION OF MAP UNITS

[Map units distinguished and interpreted on basis of morphology, texture, stratigraphic position, backscatter properties, and material associations using cycle 1 and cycle 2 synthetic aperture radar (SAR) images. Most map units distinguished as rock units with structural (tectonic) characteristic variations]

EDIFICE MATERIALS

Concentric edifice material—Smooth-textured material extending concentrically around oval-shaped edifice near lat 71°–5°S., long 192° (fig. 4), mainly to the east, where sharp margins define boundaries. Western and southern portions more uncertain, with possible embayment by mottled textured plains material (unit **pmm**). Map contains moderate density of high back-scatter narrow ridges

Unit 2—Interior surface marked by lower radar backscatter. *Interpretation:* Lava from central caldera structure underlying unit **ec1**

Unit 1—Exterior material marked by intermediate radar backscatter. *Interpretation:* Lava from central caldera structure underlying unit **ec2**

Lobate textured edifice material—Series of hummocky to smooth-textured, intermediate backscatter material showing individual lobes (commonly 20–30 km diameter) most of which extend from central edifices near lat 52° S., long 222–224° (Raskova Pateræ) and overlie regional plains material (unit **pr**). Also exhibits high backscatter lineations spaced 10–50 km apart. *Interpretation:* Overlapping lavas associated with central calderas of Raskova Pateræ

PLAINS MATERIALS

Mottled textured plains material—Often semicircular to oval-shaped, intermediate backscatter material overlying regional plains material (unit **pr**). Shows slightly hummocky texture, with margins more diffuse than, for example, mottled ridged plains material (unit **pmm**); may exhibit some mottling within larger portions and may encompass several small units (for example, dome fields (unit **df**) at lat 66.5° S., long 183°). *Interpretation:* Probable sites of volcanic (explosive) activity, with hummocky, locally mottled texture possibly resulting from the spatial resolution of SAR images of volcanic centers and (or) volcanic ejecta

Lobate plains material—Very high backscatter, digitate to lobate material overlying regional plains material (unit **pr**); usually well defined, lobate margins, although some margins may be diffuse and interspersed with mottled, lower backscatter splotches or ridges (or both). Stream-lined nature of some portions resembles crater flow material (unit **cf**). Type locality is Sicasia Planitia (lat 52° S., long 151°), which occurs at easternmost extent of map area (fig. 4). *Interpretation:* Isolated lava flow remnants, type locality represents lava flows at terminus of tectonovolcanic region west of map area

Irndr plains material—Intermediate backscatter plains material apparently emanating from the Irndr highland area to the north of the map area. Occurs only at lat 50.5° S., long 212.5° and consists of several regional plains material (unit **pr**). *Interpretation:* Large lava flows originated from now buried basins in Irndr Regio, north of map area; alternatively, early-stage Piva Pateræ and (or) Amenc Cinnga flows

Regional plains material—Mainly smooth-textured material (low to intermediate backscatter) exhibiting semilinear or semiparallel high backscatter ridges (or both), most often spaced 10–50 km apart. Embays fracturing, deformed, north-south Tinoe belts in center of map area (Sedna Dorsa) show linear to semilinear concentrations of closely spaced (<20 km) high backscatter, positive relief ridges and (or) lineaments. Southeastern part of map area (Nuptadi Planitia) shows a weblike network of semiconcentric to sinuous ridges resulting in a reticulate fabric. Contains many impact craters (fig. 5). *Interpretation:* Corrugated ridges and lineaments in mottled ridged plains material (unit **pmm**), and undifferentiated plains material (unit **pu**). *Interpretation:* Volcanic mantle units associated with major, regional rifting events, later tectonically warped or deformed by compressional forces, possibly related in places to corona formation. Smooth-textured interior areas represent lavas unaffected by ridge formation; ridged belt areas represent intense deformational (compressional) zones of overlapping wrinkle ridges and smooth ridges with minor fracturing

Undifferentiated plains material—Intermediate backscatter plains material with few patches of low backscatter material mainly in north-central part of map area (type locality; lat 51.5° S., long 209°). Overlain by regional plains material (unit **pr**). *Interpretation:* Older lava originated from Irndr Regio, north of map area, possibly from southern rim of corona at lat 47.5° S., long 209°

Mottled ridged plains material—High to intermediate backscatter plains occurring within regional plains material (unit **pr**). May have low backscatter sinuous to linear channellike features (or both) that are commonly less than 1 km wide and 1 km deep; may exhibit semilinear ridges that cross both this unit and unit **pr**. May occur as large contiguous units or as patterns of "split-bull" material with sharp to gradational edges. Composition relations difficult to discern, but regional plains material (unit **pr**) and (or) lobate textured edifice material (unit **ect**) appear to have embayed this unit. *Interpretation:* Old volcanic deposits, including lava flows, some channelized. Deformed by later ridges, contemporaneous with ridges of regional plains material

Corrugated ridged plains material—Complicated mixture of narrow high backscatter ridges or curvilinear segments with plains wrinkle ridges. May be embayed or overlain by regional plains material (unit **pr**), smooth arcuate ridge and groove material (unit **rga**), and arcuate ridge material (unit **rsa**). Embays tessera material (unit **t**) in places. Occurs only in center of map area, between lat 66° and 68° S., and north-central part of Kibh Nu Dorsum (at 68° S., long 207°; fig. 5). *Interpretation:* Compressionally deformed older plains material, or possibly the central portion of former corona complex with flooded margins and deformed rims

RIDGE MATERIALS

Arcuate ridge and groove material—Curvilinear to arcuate, semiparallel ridges and grooves elevated relative to surrounding terrain. May be embayed or crosscut by lava and wrinkle ridges of regional plains material (unit **pr**). At type locality is Piva Naret Corona (lat 66° S., long 208°), which overlies corrugated ridged plains material (unit **prc**). Where not distinguished on basis of prominent features (that is, high backscatter ridges/low backscatter grooves), may also be identified by lack of surrounding wrinkle ridges associated with regional plains material (unit **pr**). *Interpretation:* Volcanically flooded corona rims

Smooth arcuate ridge material—Like arcuate ridge and groove material (unit **rga**), but encompasses smaller semiparallel, curvilinear, smooth-topped ridges. May show intervening plains units between ridges. May also show narrow ridges at bases of individual broad ridges. At type locality (lat 63° S., long 203°) overlies corrugated ridged plains material (unit **prc**). Broad ridges especially dependent on look direction and may not appear as smooth in cycle 2 as cycle 1 images. *Interpretation:* Ridge belt apices surrounded by volcanically flooded regions; alternatively, corona rim remnants

HILLY MATERIALS

Dome fields—Clusters of small (<20 km diameter) semicircular positive relief materials. Boundary defined where density is too high for consistent use of "small shield" map symbol. May overlap into other unit boundaries. Rarely, lobate material extends radially from small central edifice. *Interpretation:* Fields of volcanic domes, rarely with associated lava flows

Tessera material—High backscatter, relatively high relief small areas showing multiple ridges (commonly intersecting) in preferentially one and rarely more than one direction. Intervening plains material grouped within this unit. *Interpretation:* Flooded former corona, tessera, or ridge belt material (or all)

CRATER MATERIALS

Crater flow material—Intermediate to very high backscatter, smooth to hummocky-textured material extending from crater showing lobate edges. May show some flow banding and gradational backscatter intensity within the unit, with slightly hummocky texture nearer crater. Commonly exhibits radar-bright splotches and backscatter sinuous streaks or channels for both may exist. Most material appears to follow topography, and some margins abut low ridges. *Interpretation:* Fluidized ejecta blanket outflow materials with channels, with possible incorporation of other lithologies as crater formed

Crater material—High to intermediate backscatter material with hummocky to speckled textures, radiating from crater with sharp to gradational distal boundaries overlying low backscatter plains material. Material may not surround symmetrically entire crater, and may form individual arms or lobes radiating from crater rim. May form transverse ridges concentrically to crater and gradational contacts with plains or crater flow material (unit **cf**). May include small patches of underlying plains. May include low to intermediate backscatter speckled regions within or at distal ends of hummocky radiating material, gradational with surrounding plains. Also includes smaller floor, walls, and rim. May include central, elevated, blocky region, or concentric, usually incomplete elevated rings with symmetric aprons of lower backscatter material at base. *Interpretation:* Impact crater and associated primary and secondary ballistic ejecta with minor fluidization. Distal ejecta may extend diffusely onto underlying plains, possibly via atmospheric entrainment of ejecta fines. Crater peak may form as single uplifted, blocky surface, or as peak-ring structure associated with impact event

Contact—Dashed where approximately located, indefinite, gradational, or inferred; dotted where concealed/buried; queried where uncertain

Fault, fracture, or fracture—Origin uncertain

Ridge crest

Narrow (wrinkle) ridge

Broad, smooth ridge

Trough

Small, elevated plateau

Scarp base—Barb points downslope; dashed where approximately located, indefinite, gradational, or inferred; queried where uncertain

Flow front—Barbs on downslope side; queried where uncertain

Flow direction

Channel (small)—Three dots where structureless or indefinite

Crater material—Hachure(s) on rim crests

Small shield (less than 20 km across)

Large edifice (20–50 km across)

Steep-sided edifice 20–50 km—Dotted where concealed/buried

Wind streaks (arrow points in inferred wind direction)

Small, diffuse covering of variable backscatter material. Visibility of underlying material (ridges and lineaments) may vary with look angle. Boundaries can be poorly defined or gradational with surrounding plains. High (look direction) backscatter material can contain cycle 1 or cycle 2 (high) backscatter material, especially on or at bases of ridges

Marked by intermediate to low backscatter in cycle 1 and cycle 2, although variable with look angle. *Interpretation:* Deposits of fines, often associated with impact-related small scale ejecta deposited/reworked

Marked by high to intermediate backscatter visible only in cycle 1 images. *Interpretation:* Variable thickness aeolian deposits forming dunes or ripples with east-facing lee sides composed of small-medium-scale fines

Marked by high to intermediate backscatter visible only in cycle 2 images (restricted to region south of central Guan Daosheng near lat 63° S., long 182°). *Interpretation:* Variable thickness aeolian deposits forming dunes or ripples with west-facing lee sides composed of small-medium-scale fines

Marked by high to intermediate backscatter visible in both cycle 1 and cycle 2 images. *Interpretation:* Variable thickness aeolian deposits forming symmetric dunes

The Magellan Mission

The Magellan spacecraft orbited Venus from August 10, 1990, until it plunged into the venusian atmosphere on October 12, 1994. Magellan had the objectives of (1) improving knowledge of the geologic processes, surface properties, and geologic history of Venus by analysis of surface radar characteristics, topography, and geomorphology and (2) improving knowledge of the geophysics of Venus by analysis of venusian gravity.

The Magellan spacecraft carried a 12.6-cm radar system to map the surface of Venus. The transmitter and receiver systems were used to collect three datasets: synthetic aperture radar (SAR) images of the surface; passive microwave emissivity and reflectivity; and venusian gravity. Because of the unprecedented power at small angles of incidence, which were processed to yield altimetric data. Radar imaging and altimetric and radiometric mapping of the venusian surface were done in seven cycles: 1, 2, and 3, from September 1990 until September 1992. Ninety-eight percent of the surface was mapped with radar resolution of approximately 120 meters. The SAR observations were projected to a 75-m nominal horizontal resolution. These full-resolution data compose the image base used in geologic mapping. The primary polarization mode was horizontal-transmit/horizontal-receive (HH). In some areas, cross-polarized (horizontal transmit/vertical receive) backscatter sense. Incidence angles varied from about 20° to 45°.

High-resolution Doppler tracking of the spacecraft was done from September 1992 through October 1994 (mission cycles 4, 5, 6). Because of the Doppler tracking, nearly observations from about 950 orbits were obtained between September 1992 and May 1993, while Magellan was in an elliptical orbit with a periapsis near 175 kilometers and an orbit period of 3.2 hours. Observations in an additional 1,500 orbits were obtained following orbit-circularization in mid-1993. These data exist as a 75° by 75° harmonic field.

Magellan Radar Data

Radar backscatter power is determined by the roughness of the surface at a broad range of scales and by the intrinsic reflectivity, or dielectric constant, of the material. Topography at scales of several meters and larger can produce quasi-specular echoes if the surface is tilted toward the spacecraft or quasi-diffuse echoes perpendicular to the incident beam. This type of scattering is most important at very small angles of incidence, because normal surfaces appear to be flat at small angles. Rough surfaces also scatter radar energy in areas of steep slopes, such as ridges or rift zones, where favorably tilted terrain can produce very bright signatures in the radar image. For small angles of incidence, diffuse echoes from rough surfaces are comparable to the radar wavelength are responsible for variations in the SAR return. In either case, the echo strength is also modulated by the reflectivity of the surface material. The density of the upper few wavelengths of the surface can have a significant effect on the echo strength. Areas of low density, such as deep, dry, fine-grained soil or very light SAR echoes from virtually all areas about that critical elevation.

The measurements of passive thermal emissivity at wavelengths, though of much lower spatial resolution than the SAR data, are more sensitive to changes in the dielectric constant of the surface than to roughness. As such, they can be used to distinguish areas of similar roughness but different composition or density on very bright SAR echoes from virtually all areas about that critical elevation.

The altimetric measurements of surface topography and slope, which yield the horizontal scale of the surface, are used to derive the corresponding images of ridges and fractures elevated relative to the surrounding terrain and embayed or crosscut by lavas and rock-mantled plains material. The arcuate ridge and groove unit is interpreted as a type of volcanically flooded corona rim. A similar unit is associated with mottled ridged plains material (unit **rsa**), which also shows arcuate ridges and groove, smooth-topped ridges. this material may represent either ridge belt apices surrounded by volcanically flooded regions or corona rim remnants in places.

Mottled ridged plains material (unit **pmm**) represents old volcanic deposits, some with channelized lava flows, which deformed contemporaneously with wrinkle ridge formation in the regional plains material. This material often occurs in "splotchy" patterns with sharp to gradational edges making superposition relations with regional plains material (unit **pr**) difficult to discern. However, in several areas, regional plains material overlies mottled ridged plains material. Undifferentiated plains material (unit **pu**) occurs only in the north-central part of the map area (type locality at lat 51.5° S., long 209°). This material is distinguished by its embayment by regional plains material and higher backscatter. It appears to be older lavas originated from the southern rim of a corona at lat 51° S., long 209°.

Regional plains material (unit **pr**) comprises the majority of the map area and represents a significant period of volcanic flooding and tectonic activity in this region. Both structurally smoother areas and ridge belts are incorporated in this unit. This region therefore referred to as the "mottled wrinkle ridge plains" wrinkle ridge deformation; whereas ridge belt areas represent intense deformational (compressional) zones of overlapping wrinkle ridges and smooth ridges with minor fracturing. Nearly all other plains material exposures are in contact with the regional plains material, although not necessarily with each other.

Channels are small volcanic conduits that are shaped as sinuous rilles (unit **df**) occur among most plains materials throughout the stratigraphic column. They are distinguished by their circular shape, relatively high relief (as evidenced by backscatter on their radar-facing sides), and by their radial distribution from the source interpreted as summit pits. Rarely, flow material is observed surrounding individual domes. The viability of these features can depend on look direction and the backscatter contrast difference between the dome and surrounding material. It is difficult to interpret the age of domes that occur within stratigraphically older materials (for example, unit **prc**), because they do not show clearly either the structural disruption characteristic of the unit or younger flow materials. Though a few older cones do appear to have been flooded contemporaneously with older units by younger regional plains material (for example, lat 65.78° S., long 203.13°), others occur as completely younger features that post-date regional plains material into older units (for example, lat 67.5° S., long 209.8°).

Mottled textured plains material (unit **ptm**) is often semicircular to oval-shaped material up to 40 km across that may coalesce into irregularly shaped regions >100 km across. It has been deformed by wrinkle ridges contemporaneously with those in the regional plains material. Unit **ptm** shows a slightly hummocky texture with intermediate, mottled backscatter and margins more diffuse than mottled ridged plains material (unit **pmm**). It is interpreted as sites of volcanic inspiloose? activity, with the hummocky, broken textures suggestive of many small Below spatial resolution of SAR images/volcanic centers and (or) volcanic ejecta (for example, Ila). This unit may represent one of the last stages of volcanic activity after formation of the regional plains material.

Irndr plains material (unit **pl**) is low backscatter material that occurs at lat 52.5° S., long 212.5°. It appears to have emanated from the Irndr highland area to the north of the map area and covers regional plains material. This unit may represent extensive, early-stage lava flows originated from now buried basins in Irndr Regio, north of map area (lat 46.5° S., long 214.5°) or fissure flows from Irndr Regio.

Lobate plains material (unit **pl**) is very high backscatter (fig. 6A), digitate to lobate material interpreted as lava flows overlying the regional plains material. The flows at the type locality, Sicasia Fluctus (lat 52° S., long 181°), are interpreted to have originated from a tectonovolcanic region west of the map area. The streamlined nature of some flows is shown by the narrowly-spaced lineations and by symbols rather than through mapping of units. As such, significant structural features such as Saule Dorsa are not mapped as geologic units, but rather as intensely deformed material (units of former plains material).

Coronae such as Piva Naret and Amenr are not mapped as units, although their rims are distinguished as units (unit **rga**, **rsa**). The boundaries of artificial units are mapped to the centroids of the materials. Areas of overlapping regions between different cycles (see fig. 1). Some regions have anomalously higher (or lower) backscatter in one cycle compared to another. These are distinct from regions in which backscatter differences between cycles are more normal for geologic (fig. 6B).

Photographic and digital versions of the SAR images from cycles 1 and 2 provide the main tool for geologic mapping. Photographic (1:1,000,000 scale) and digital (Compact Disc-Read Only Memory [CD-ROM] Standard Archive Format Record [F–MDR]) images (sampled to 75 m/pixel) are used where available for detailed study of particular features, whereas compressed images (C1–, C2–, and C3–MDR's) provide regional perspectives, including regions beyond the limit of the map area. Photographic versions of USGS-produced full-resolution maps (FMAP's) allow detailed comparison of widely spaced regions at full Magellan resolution and (or) stereoscopic analysis by using overlapping coverage. Locations of small features in a valley between two ridges, possibly provide a strip for windblown materials.

Lobate textured edifice material (unit **edz**) is interpreted as regional plains material and is disrupted by wrinkle ridge formation contemporaneous with that of the regional plains material. It includes numerous overlapping lavas, often the planet. Lobate textured edifice material (unit **edz**) is interpreted as regional plains material and is disrupted by wrinkle ridge formation contemporaneous with that of the regional plains material. It includes numerous overlapping lavas, often the planet.

Magellan altimetry has lower spatial resolution than SAR but is nonetheless vital to understanding the present topography of the region, and for altimetric and radiometric mapping. The altimetric data for this map. The first is USGS-produced "synthetic stereo" photographic C1–MDR images in which parallax is introduced by shifting pixels depending on their altitude in a registered Magellan topographic image. Stereo viewing of SAR images having similar illumination geometry but 30° to 40° look-angle difference is valuable for determining relative elevations between adjacent regions. Placement of structural symbols for ridges and troughs often is based on comparison of the synthetic stereo images with topography for the region. The second product is a synthetic perspective image created by draping SAR images over topography (figs. 4, 5). These images provide an additional means of visually comparing the distribution of stratigraphic units and structural features with topography. Though both of these products are subject to artifacts resulting from the mismatch in spatial resolutions between SAR and altimetric data, they are extremely valuable for relief within the SAR coverage and greatly minimizes these effects.

The other radar datasets (emissivity, reflectivity, and root mean square (rms) slope available on the GxDR CD-ROM [National Aeronautics and Space Administration, 1993]) help characterize the surface properties of units that have been mapped using SAR data. Radar property information (table 2) was not used in the construction of the order of impact cratering events (with the exception of Barrymore).

Mean emissivity and reflectivity images (Campbell and others, 1992) have a spatial resolution near lat 56.5° S., long 192°, and reticulate patterns of wrinkle ridges occur near lat 56° S., long 217° and near lat 71.5° S., long 220°. Using the techniques of McGill (1993, 1994) to determine stratigraphic relations between wrinkle ridges and impact craters, it is interpreted that the wrinkle ridges are younger than the craters. Where over the course of the 8-month time period between cycle coverage) one would expect those surface property values to be different. Some of the variations in reflectivity and emissivity that are observed over the mapped area correspond to differences in the geologic units. Comparison of Goldstone and Magellan radar data in the equatorial plains of Venus: Journal of Geophysical Research, v. 98, p.5479–16,291.

Phillips, R.J., Arvidson, R.E., Boyce, J.M., Campbell, D.B., Guest, J.E., Schaber, G.G., and Soderblom, L.A., 1991, Impact craters on Venus: Initial analysis from Magellan: Science, v. 252, p. 288–297.

Plaut, J.J., and Arvidson, R.E., 1992, Comparison of Goldstone and Magellan radar data in the equatorial plains of Venus: Journal of Geophysical Research, v. 97, p.16,279–16,291.

Plaut, J.J., Saunders, R.S., Stofan, E.R. Kirk, R.L., Schaber, G.G., Soderblom, L.A., Ford, P.G., Pettengill, G.H., Campbell, D.B., Stacy, N.J.S., Arvidson, R.E., and Greeley, Ronald, 1992, Anomalous scattering behavior of selected impact "parabolic" features: Magellan cycle-two/cycle-three comparisons: Paper presented to the International Colloquium on Venus: Lunar and Planetary Institute Contribution No. 789, p. 92–93.

Schaber, G.G., Kirk, R.L., and Strom, R.G., 1996, Data base of impact craters on Venus based on analysis of Magellan radar images and altimetry data: U.S. Geological Survey Open-File Report 96–688 [revision of USGS Open-File Report 95–563 of the same title].

Schaber, G.G., Strom, R.G., Moore, H.J., Soderblom, L.A., Kirk, R.L., Chadwick, D.J., Dawson, D.D., Gaddis, L.R., Boyce, J.M., and Russell, Joel, 1992, Geology and distribution of impact craters on Venus: What are they telling us?: Journal of Geophysical Research, v. 97, p. 13,257–13,301.

Schultz, P.H., 1992, Atmospheric effects on ejecta emplacement and crater formation on Venus from Magellan: Journal of Geophysical Research, v. 97, p. 16,183–16,248.

Squyres, S.W., Janes, D.M., Baer, Gidon, Bindschadler, D.L., Schaber, Gerald, Sharpton, V.L., and Stofan, E.R., 1992, The morphology and evolution of coronae on Venus: Journal of Geophysical Research, v. 97, p. 13,611–13,634.

Stofan, E.R., Sharpton, V.L., Schubert, Gerald, Baer, Gidon, Bindschadler, D.L., Janes, D.M., and Squyres, S.W., 1992, Global distribution and characteristics of coronae and related features on Venus: Implications for origin and relation to mantle processes: Journal of Research, v. 97, p. 13,347–13,378.

Strom, R.G., Schaber, G.G., and Dawson, D.D., 1994, The global resurfacing of Venus: Journal of Geophysical Research, v. 99, p. 10,899–10,926.

Tanaka, K.L., 1994, The Venus geologic mappers' handbook (2d ed.): U.S. Geological Survey Open-File Report 94–438, 50 p.

Weitz, C.M., Plaut, J.J., Greeley, Ronald, and Saunders, R.S., 1994, Dunes and microdunes on Venus: Why they were so low found in the Magellan data?: Icarus, v. 112, p. 282–295.

Wilhelms, D.E., 1990, Geologic mapping, *in* Greeley, Ronald, and Batson, R.M., eds., Planetary mapping: New York, Cambridge University Press, p. 208–260.

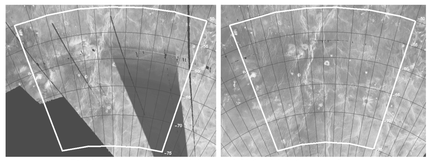

QUADRANGLE LOCATION

Photomosaic location is shown in the western hemisphere of Venus. An outline of 1:5,000,000-scale quadrangles is provided for reference.

Prepared on behalf of the Planetary Geology Program, Solar System Exploration Division, Office of Space Science, National Aeronautics and Space Administration
Edited by Derrick Hirsch; cartography by Michael E. Dingwell and Darlene A. Carpainter
Manuscript approved for publication June 19, 1997

Figure 1. Comparison of cycle 1 (left; left-looking) and cycle 2 (right; right-looking) coverage for Barrymore quadrangle and surrounding regions. North is toward the top in both images. Grid is shown in 5-degree latitude and longitude increments. Lambert projection centered at lat 63.5° S., long 210°. Map area boundary is outlined in white.

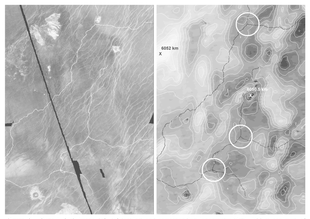

Figure 2. Cycle 1 SAR image (left; left-looking) and corresponding topography (right; 100-m contours) of northwestern part of map area centered at lat 55° S., long 183°. Overlain on both are tracings of canali-type channels showing three bifurcation points (within large white circles on topography image) in which orientations change from predominantly north-south to east-west directions. North is toward the top in both images. Highest and lowest elevations are marked on topography image. Image is about 750 km across.

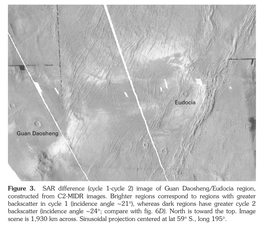

Figure 3. SAR difference (cycle 1-cycle 2) image of Guan Daosheng/Eudocia region, constructed from C2-MIDR images. Brighter regions correspond to regions with greater backscatter in cycle 1 (incidence angle ~21°), whereas dark regions have greater cycle 2 backscatter (incidence angle ~24°; compare with fig. 6*B*). North is toward the top. Image scene is 1,930 km across. Sinusoidal projection centered at lat 59° S., long 195°.

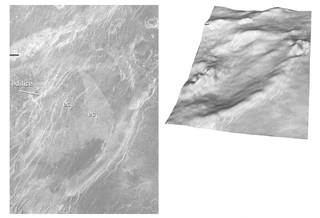

Figure 4. SAR image (cycle 2; right-looking) and accompanying synthetic perspective image created using Magellan topography of region centered near lat 71° S., long 195°, showing portions of concentric edifice material (units **ec1**, **ec2**) near a large, broad basin bounded by a sinuous ridge (Chih Nu Dorsum). Edifice left of center arrowing high backscatter ridges is 50 km long. North is toward the top. Image scene is about 420 km across.

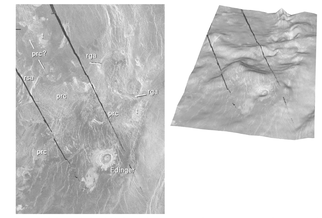

Figure 5. SAR image (cycle 1; left-looking) and accompanying synthetic perspective image of region centered near lat 62.5° S., long 202°; near center of map area, showing examples of lineaments material (unit **l**), corrugated ridged plains material (unit **prc**), smooth arcuate ridge material (unit **rsa**), and arcuate ridge and groove material (unit **rga**) of Piva Naret corona near crater Edinger (35 km diameter). North is toward the top. Image scene is about 420 km across.

STRUCTURE

The overall structure in the map area is dominated by 10 east-west compressional tectonics resulting in nearly ubiquitous north-south linear wrinkle ridge formation, (2) more intense compressional belts, such as Saule Dorsa, Sedna Dorsa, and Nuptadi Dorsum, the destruction of regional material (unit **pr**), and (3) broad, smooth swells such as Nartsh and Chih Nu Dorsa (fig. 4). This deformation appears to have occurred later in the history of this area (as evidenced by the superposition of the wrinkle ridges over most of the other units) and with moderate strain (Ford and Pettengill, 1992), have unique (albeit not well constrained) surface property characteristics.

Further, it was noted that the reflectance, emissivity, and rms slope values in the majority of the map area did not change noticeably between cycles 1 and 2. If the surface materials had changed between the cycle 1 and cycle 2 data acquisition time intervals, it is interpreted that the observed differences would be evident as, for example, the Guan Daosheng/Eudocia region (fig. 3). Variations in the emissivity and rms slope values for the corresponding differences. Johnson [1992] concluded that the reasons for the backscatter differences observed for these extended deposits between cycles 1 and 2 are related to changes in surface material but rather due to surface scattering characteristics resulting from dune face and (or) ripple geometry.

GEOLOGIC HISTORY

The geologic history of Barrymore quadrangle involves early, intense tectonic deformation of precursor material prior to areally extensive plains volcanic flooding. Regional compression followed, forming ridged plains and linear ridge belts. Contractional deformation occurred after this event, with the most recent depositing extended surficial deposits affected by aeolian processes.

The oldest unit is tessera material (unit **t**), which occurs mainly in the region of the intersection between Saule Dorsa and the north-south trending Tinoe belt. Also in this region, arcuate ridge and groove material (unit **rga**), smooth arcuate ridge material (unit **rsa**), and complicated plains regions (corrugated ridged plains material (unit **prc**) and mottled ridged plains material (unit **pmm**) are found. Origin and distribution of impact craters on Venus: What are they telling us?: Journal of Geophysical Research, v. 97, p. 13,257–13,301.

Schultz, P.H., 1992, Atmospheric effects on ejecta emplacement and crater formation on Venus from Magellan: Journal of Geophysical Research, v. 97, p. 16,183–16,248.

Squyres, S.W., Janes, D.M., Baer, Gidon, Bindschadler, D.L., Schaber, Gerald, Sharpton, V.L., and Stofan, E.R., 1992, The morphology and evolution of coronae on Venus: Journal of Geophysical Research, v. 97, p. 13,611–13,634.

Stofan, E.R., Sharpton, V.L., Schubert, Gerald, Baer, Gidon, Bindschadler, D.L., Janes, D.M., and Squyres, S.W., 1992, Global distribution and characteristics of coronae and related features on Venus: Implications for origin and relation to mantle processes: Journal of Research, v. 97, p. 13,347–13,378.

Strom, R.G., Schaber, G.G., and Dawson, D.D., 1994, The global resurfacing of Venus: Journal of Geophysical Research, v. 99, p. 10,899–10,926.

Tanaka, K.L., 1994, The Venus geologic mappers' handbook (2d ed.): U.S. Geological Survey Open-File Report 94–438, 50 p.

Weitz, C.M., Plaut, J.J., Greeley, Ronald, and Saunders, R.S., 1994, Dunes and microdunes on Venus: Why were so few found in the Magellan data?: Icarus, v. 112, p. 282–295.

Wilhelms, D.E., 1990, Geologic mapping, *in* Greeley, Ronald, and Batson, R.M., eds., Planetary mapping: New York, Cambridge University Press, p. 208–260.

Figure 6. Backscatter cross sections (σ_0) versus incidence angle (cycle 1 and cycle 2) for all units in Barrymore quadrangle: *A*, Plains materials; *B*, crater materials and edifice materials; *C*, ridge materials and hilly materials; *D*, surficial materials. Values obtained using method and software of Campbell (1994, 1995). See table 2 for specific values and ancillary radar property information. Each average value is shown with plus and minus one standard deviation from average. Muhleman curve represents average Venus backscatter response (Campbell, 1995; Tanaka, 1994).

Table 2a. *Radar property data for geologic units in Barrymore quadrangle (V–59).*

[For each unit, first line is cycle 1 data, second line is cycle 2 data. Backscatter values are given as average σ_0, computed from given number of pixels in plus and minus one standard deviation (in parentheses) using the method and software of Campbell (1994). No cycle 1 coverage exists for unit **ec1**]

Unit	Latitude,Longitude	Pixel	Number scale (m)	Incidence angle of pixels	Backscatter (dB) range (degrees)
ec1	(–70.196,–69.992), (195.060,195.607)	225	8372	18.40–18.33	–8.638 (+9.902,–7.660)
ec1			8536	21.64–21.56	–9.719 (–11.095,–8.679)
ec2					
ec2	(–70.256,–70.115), (194.509,194.839)	225	3015	21.59–21.54	–10.776 (–12.129,–9.745)
ec2	(–54.964,–54.774), (188.360,188.578)	225	5520	21.87–21.82	–13.641 (–14.570,–12.546)
pr			5520	24.74–24.73	–13.936 (–15.244,–12.933)
edz	(–51.359,–51.193), (223.499,223.717)	225	5056	22.89–22.84	–11.969 (–13.491,–10.641)
edz			5056	24.99–24.98	–12.728 (–14.768,–11.340)
pmm	(–59.602,–59.448), (227.422,227.775)	225	5548	20.82–20.79	–13.957 (–15.197,–12.593)
ptm			5548	24.17–24.16	–9.500 (–12.044,–7.906)
prm	(–